NeuroImage **14,** 1327–1336 (2001)
doi:10.1006/nimg.2001.0948, available online at http://www.idealibrary.com on IDEAL®

Hemodynamic and Electroencephalographic Responses to Illusory Figures: Recording of the Evoked Potentials during Functional MRI

F. Kruggel, C. S. Herrmann, C. J. Wiggins, and D. Y. von Cramon

Max-Planck-Institute of Cognitive Neuroscience, Stephanstrasse 1, 04103 Leipzig, Germany

Received April 30, 2001

The feasibility of recording event-related potentials (ERP) during functional MRI (fMRI) scanning using higher level cognitive stimuli was studied. Using responses to illusory figures in a visual oddball task, evoked potentials were obtained with their expected configurations and latencies. A rapid stimulation scheme using randomly varied trial lengths was employed, and class-wise characteristics of the hemodynamic response were obtained by a nonlinear analysis of the fMRI time series. Implications and limitations of conducting combined ERP–fMRI experiments using higher level cognitive stimuli are discussed. EEG/fMRI results revealed a sequential activation of striate and extrastriate occipital cortex along the ventral path of object processing for Kanizsa figures. Interestingly, Kanizsa figures activated the human motion area MT. Targets resulted in activations of frontal and parietal cortex which were not activated for standard stimuli.

Key Words: **event-related potentials; functional magnetic resonance imaging; illusory figures; rapid stimulation; N1; P3.**

INTRODUCTION

Electric potentials and the hemodynamic response of the vascular system are measurable correlates of the brain's neuronal activation. The former effect, which can be measured by event-related potentials (ERP), is a direct consequence of the electrical activity of neurons and allows observation of the underlying cognitive processes on a millisecond time scale. The latter effect, recordable by functional magnetic resonance imaging (fMRI), is only indirectly linked to the energy consumption of the neuronal population and takes place on a time scale which is on the order of seconds. However, recent developments in experimental techniques and data analysis have shown that hemodynamic responses are indeed modulated by the experimental stimulation and carry information about the underlying processes at least on a 100-ms time scale [6, 9, 28, 40].

The localization of an activation by ERP source analysis suffers from poor spatial resolution and the theoretical problem of providing only inexact solutions. Here, fMRI is better able to localize brain activations at a high spatial resolution. A combination of both techniques is a very attractive aim in neuroscience, and a number of research groups have taken up the challenge. Most studies so far were performed as separate experiments (i.e., ERP and fMRI recordings at different times), and results were registered and combined by data processing (e.g., [34, 38, 43]). Especially for cognitive stimuli, it is impossible to control whether a subject performs in the same manner in both experiments (e.g., a response may habituate due to stimulus repetition). On the other hand, a combined measurement (i.e., recording ERPs during fMRI scanning) reveals a number of delicate technical problems: gradients applied during fMRI scanning induce voltages which are much higher than the brain's response and thus interrupt electroencephalogram (EEG) acquisition; the so-called cardioballistic effect overlays a pulse-synchronous signal on the EEG, most likely due to pulsation-induced small head and wire movement in the field; electrodes and leads of the EEG setup interact with the fMRI scanning process.

A number of research groups have worked on the technical details of the problems of recording an EEG in the magnetic field [1, 2, 8, 13, 21, 22, 26, 32, 37] and recently have demonstrated the feasibility of recording visual evoked potentials during fMRI scanning [3, 29, 4]. To address interesting questions in cognitive neuroscience, it is necessary to develop experimental strategies and evaluation techniques for conducting experiments using cognitive stimuli and to demonstrate that results are (at least) equivalent to those from separate measurements.

One of the main problems is the low signal-to-noise ratio (SNR) of ERP experiments, which typically require 50–100 repetitions per stimulus class. To obtain a similar ERP quality under the interfering measuring conditions of combined experiments, we estimate that two to three times the number of trials must be con-

1053-8119/01 $35.00

ducted—even a simple factorial design includes 500–1000 trials. Given the rather uncomfortable and confined situation for a subject in the MR tunnel, the duration of an fMRI experiment (excluding preparatory scans) is limited to typically 45 min. Thus, the trial length may not exceed 2.5–5 s, which leads to strongly overlapping hemodynamic responses. Burock *et al.* [7] demonstrated that disentangling responses from rapid presentation rates is possible when using a randomly varied trial length.

The purpose of this study is to demonstrate the feasibility of conducting combined ERP–fMRI experiments under cognitive stimulation. We employ a well-studied cognitive visual oddball task using illusory figures for which EEG and MEG responses are known [17, 18]. PET and fMRI experiments with illusory figures have also identified which neural generators are involved in their perception, but the temporal sequence of their activation has remained unclear so far [20, 36, 31]. To investigate the temporal interplay of the neural substrates of illusory figure perception and target detection, we combined EEG and fMRI recording. The experimental design incorporates four conditions with 225 repetitions each and a randomly varied trial length of 2–3.5 s. Methods for post hoc artifact correction are described, as well as a nonlinear model for disentangling the strongly overlapping hemodynamic responses. ERP and fMRI results from this experiment correspond well with those from previous separate measurements. Finally, additional benefits of conducting a combined experiment are discussed.

SUBJECTS, EXPERIMENTAL SETUP, AND DATA EVALUATION

Twelve healthy persons took part in this study (5 female, 7 male, mean age 24.8 years, range 22–30 years). All subjects had previous experience as test persons in EEG and fMRI studies. None of the subjects had participated in experiments employing Kanizsa figures before. They received a nominal compensation for their effort. All subjects gave informed consent in accordance with guidelines set by the Max-Planck-Institute.

Subject Setup

Conventional plastic-coated Ag/AgCl electrodes with iron-free copper leads of 60 cm length were fixed on the subject's scalp by a stretchable plastic cap. Electrodes were mounted at all positions of the international 10/20 system except Pz, where leads left the cap. The reference electrode was placed close to the nasion on the forehead. Electrode positions were tracked using a Polhemus Fastrak 3D digitizer. Cables were twisted pairwise and led through a flexible silicon tube to the EEG amplifier located above the subject's head, i.e., along the body axis in the scanner tunnel. In order to minimize movements, the subject's head was restrained using cushions. Cables and amplifier were fixed to the gantry by tape and weighed down by rice bags. Subjects wore mirror glasses in order to perceive the visual stimulation.

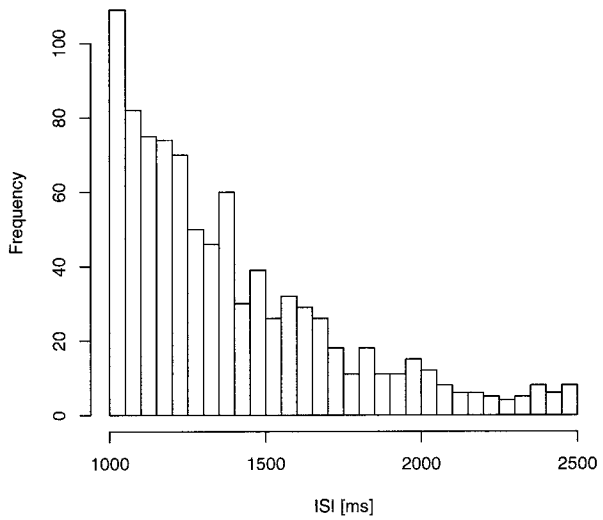

FIG. 1. Histogram of the interstimulus interval (ISI) used in the rapid randomized design. The histogram follows a geometrical distribution corresponding to ISI = 1000 − 500 × log (*d*), $d \in [0.04979;1]$.

Stimulation

We used Kanizsa figures and non-Kanizsa figures (see Fig. 2) as stimulus material [17]. Stimuli consisted of either three or four inducer disks, which we will consider the shape feature and either constituted an illusory figure (Fig. 2, top row) or not (Fig. 2, bottom row). Stimuli were presented for 1000 ms, followed by randomized interstimulus intervals (ISI) of 1000 to 2500 ms. The ISI duration followed an exponential distribution corresponding to ISI = 1000 − 500 × log(*d*), $d \in [0.04979; 1]$ (see Fig. 1, refer to [23] for a thorough discussion).

Figures were displayed in black on a white background with a black fixation cross in the center. Stimuli subtended a visual angle of 4.28° including inducer disks, while the induced illusory figures (Fig. 2, top) subtended 2.86°. Fixation crosses were displayed foveally (0.02°). The ratio of the inducing line ends and the side length of the illusory figures was 1/4. The ERTS package (Berisoft GmbH, Frankfurt, Germany) was used for display programming and recording of behavioral reaction times. The stimulation pattern was projected onto a screen in the scanner tunnel from a LCD projector located outside the scanner room.

A block of 20 trials (approx 50 s) was followed by a 10-s display of the fixation cross alone. Forty-five blocks were recorded in three experimental runs (a total of 900 trials). A single trigger pulse was sent from the MR console to the stimulation PC to start an experimental run. Conditions Kanizsa square (KS),

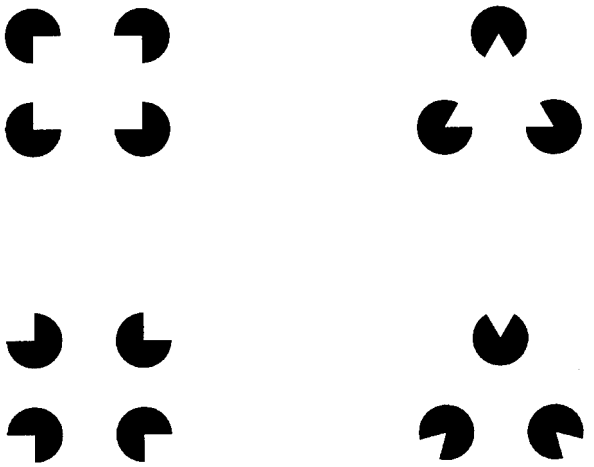

FIG. 2. Stimulus material used in the experiment: in the top row, Kanizsa square and triangle, below, non-Kanizsa square and triangle.

Kanizsa triangle (KT), non-Kanizsa square (NS), and non-Kanizsa triangle (NT) were presented equiprobably and randomized across subjects and runs. The KS served as the target condition. Subjects were instructed to press a button with their right middle finger when a target appeared ($P = 0.25$) and to press another button with the right index finger for all other conditions ($P = 0.75$).

EEG Recording and Data Evaluation

A commercially available MR-compatible system (Schwarzer, Munich, Germany) was used for EEG recording. The battery-powered amplifier located in the scanner tunnel was connected via a 20-m fiber-optic link to a standard PC equipped with a digital signal processor (DSP) board in the MR console room. The DSP board received trigger input from the stimulation PC which was recorded with the biosignals. The amplification factor of the system was 10,000×, with a bandwidth of 0.073–70 Hz. Biosignals were sampled at 500 Hz using a unipolar recording with nasion as reference at the following positions of the international 10/20 system: Fp1, Fp2, F3, F4, C3, C4, P3, P4, O1, O2, F7, F8, T3, T4, T5, T6, Fz, Cz, and Cb2 (ECG trace).

Collected data were analyzed offline in a series of steps: Low- and high-frequency components of the signal were removed using a Hamming-weighted band-pass filter with a pass-band of 0.8–30 Hz. Artifacts from MR gradient pulses were detected in the summed signal. If the slope of this signal exceeded 25 μV/ms, the subsequent interval of 400 ms was marked for exclusion. The cardioballistic artifact was corrected by a trial-wise template-based approach described in detail elsewhere [29]. Finally, the corrected EEG was averaged across subjects in a period of −100 to +600 ms relative to stimulation onset, selecting periods with correct responses and specific conditions only.

fMRI Scanning and Data Evaluation

Functional imaging was performed using a Bruker Medspec 30/100 3.0-T MR system equipped with a birdcage quadrature coil. An in-house EPI implementation allowed the acquisition of the slices to be collected together at the beginning or the end of the TR time, thus providing long pauses during which no MR signals were being recorded for the collection of the EEG data. Sequence parameters were TE 30 ms, TR 1500 ms between successive acquisitions of the same slice. Five axial slices were acquired with thickness 6 mm, 2-mm gap, 19.2-cm FOV, 64 × 64 matrix with 100-kHz sampling. Slices were oriented parallel to the AC-PC line in the sagittal plane approx at z coordinates −13, −5, +3, +43, and +50 mm. The time period during which the images were acquired was 270 ms, leaving a period of 1230 ms for MR relaxation and EEG acquisition.

Collected fMRI data were analyzed offline in a series of steps: Time series were corrected voxel-wise for their EPI acquisition delay. *Subject movements* were corrected in 2D (two translational and one rotational parameter) within and between both scans [12]. *Baseline filtering* was achieved by estimating the baseline using low-pass filtering in the temporal domain (cut-off 0.0125 Hz) and subtraction of the result from the data [27]. *Functional activation* was detected by voxel-wise univariate regression analysis. The regression analyses were designed to distinguish (1) task-related activation (KS, KT, NS, NT) from baseline (display of fixation cross alone), (2) target- (KS) vs nontarget- (KT, NS, NT) related activation, (3) activation related to Kanizsa (KS, KT) vs non-Kanizsa figures (NS, NT), and (4) activation related to squares (KS, NS) vs triangles (KT, NT). In all designs, the first two time steps of each stimulus and baseline period were excluded from analysis as transition phases. In addition, the first five time steps of each scan were excluded due to their magnetic nonequilibrium. In designs (2)–(4), the baseline period was excluded as well. The design matrix was shifted by 5.5 s to match the lag of the hemodynamic response. The F scores obtained were corrected for the effective degrees of freedom by analyzing the temporal autocorrelation [44] and converted into Z scores. Z-score maps were registered with a T_1-weighted high-resolution MR data set of the same subject and transformed into Talairach space and averaged within the subject group. The resulting Z-score map was thresholded by 4 and activated regions were assessed for their significance on the basis of their spatial extent [11] using a region-wise probability threshold of $P < 0.05$. For graphic display, significantly activated brain areas were color-coded and overlaid onto the group-averaged anatomical high-resolution data set.

In order to evaluate activated regions quantitatively, a nonlinear model was adapted to the time series. Referring to a recent description in this journal [30],

TABLE 1

Responses and Reaction Times for Individual Subjects

	Response			Target		Nontarget	
Subject	Correct	Incorrect	Missed	Mean (ms)	Std dev (ms)	Mean (ms)	Std dev (ms)
1	837 (93.0%)	50	13	601.9	126.2	560.2	149.5
2	876 (97.3%)	24	0	737.2	91.0	727.3	129.5
3	892 (99.1%)	8	0	743.1	78.0	673.9	102.7
4	884 (98.2%)	11	5	652.9	95.8	610.8	140.1
5	883 (98.1%)	3	14	782.9	142.4	711.9	164.7
6	888 (98.6%)	12	0	639.1	74.6	600.7	78.2
7	877 (97.4%)	18	5	807.4	94.3	710.8	137.0
8	893 (99.2%)	6	1	662.6	77.2	612.3	84.8
9	879 (97.6%)	21	0	732.7	94.2	664.0	90.2
10	889 (98.7%)	9	2	781.8	85.3	718.0	93.3
11	897 (99.6%)	2	1	765.8	73.8	688.6	84.7
12	520 (57.7%)	0	380	796.3	112.5	744.4	163.7

we deliberately keep the discussion of our method short. Each hemodynamic response due to a single stimulus is modeled by a Gaussian function. We assume that each stimulus of a given class elicits the same response and that subsequent stimuli add linearly [5]. This defines the model of the time series y as

$$y = \sum_{s} \sum_{t=0}^{t_{\max}} (g_{c(s)} \times \exp(-((t - l_{c(s)})/d)^2) + o, \qquad (1)$$

where the parameters of the Gaussian function are called g, gain; l, lag; d, dispersion, and o, offset. The inner sum models the hemodynamic response due to a single stimulus in the time interval $t \in [0,t_{\max}]$ lasting from stimulation onset for an arbitrary time (here, $t_{\max} = 12s$). The outer sum runs over all trials s of the experiment, with $c(s) \in \{KS, KT, NT, NS\}$ referring to the stimulus class. Note that the dispersion and the offset were assumed class-independent. The signal is sampled at integral multiples of TR (the actual time points of measurements), and the slice-dependent acquisition delay of the EPI protocol was taken into account.

First, regions-of-interest (ROIs) were determined by computing a regression analysis in single subjects as described above, measuring the effect of stimulation periods (KS, KT, NS, NT) vs fixation point display. In the resulting individual Z-score maps, we defined regions of six four-connected, suprathreshold ($Z \geq 6$) voxels around local maxima and selected those regions whose position most closely resembled regions found in the group analysis (see Table 2). The time series for a ROI was obtained by averaging voxel intensities at a given time point. Note that spatiotemporal correlations were neglected.

Parameters of the model function were optimized using Powell's algorithm [39]. Ten parameters (gain and lag for each class, class-independent dispersion and offset) were determined from a time series of 1800 points. For inter-subject comparisons, relative gain values were computed for each subject and each ROI: $rg_c = g_c/\Sigma_c g_c$. Lag times were normalized by subtracting the individual lag of a ROI within the area striata (AS).

RESULTS

Behavioral Results

Reaction times and responses were recorded along with the stimulation. Results are collected in Table 1.

Subject 12 was excluded from further evaluation. Reaction times for target conditions were significantly higher for target trials (725.3 ± 68.9 ms) than for nontarget trials (668.5 ± 59.2 ms, $P < 1 \times 10^{-8}$).

Functional Imaging Results

Quantitative results from the evaluation of the fMRI group data are compiled in Table 2 for selected brain regions and shown overlaid onto the group-averaged anatomical data set in Fig. 3. Results are interpreted as follows:

- During stimulation (conditions KS, KT, NS, and NT vs fixation point) activations are found at expected locations (see Table 2 and Fig. 3, top row): the left motor cortex (MCL), the supplementary motor area (SMA), the left and right superior parietal lobe (SPLL, SPLR), and bilaterally the lateral occipital gyri at anterior, middle, and posterior locations (AOGL, AOGR, MOGL, MOGR, POGL, POGR). Interestingly, the periphery of the AS and Heschl's gyrus is suppressed on both sides.
- The evaluation of target (KS) vs nontarget (KT, NS, NT) conditions revealed a bilateral activation of the middle frontal gyri (MFGL, MFGR) and SPLL and SPLR and a stronger activation of MCL and SMA (Fig. 3, second row). The periphery of AS exhibits a relative activation (i.e., a less pronounced suppression). No activations of extrastriate visual cortex were found for target stimuli.

TABLE 2

Selected Activation Foci for All Stimuli vs Fixation, Target vs Nontarget conditions, Kanizsa vs non-Kanizsa Figures, and Square vs Triangle Figures

	Coordinates			(KS, KT, NS, NT) vs fixation		(KS) vs (KT, NS, NT)		(KS, KT) vs (NS, NT)		(KS, NS) vs (KT, NT)	
Anatomical location	x	y	z	Integral	Z_{max}	Integral	Z_{max}	Integral	Z_{max}	Integral	Z_{max}
Motor cortex left	−38	−19	53	40,181	11.81	26,305	8.97	21,618	9.10	14,428	8.35
Supplementary motor area	−5	1	54	5,787	10.16	6,788	6.24	3,586	6.74	1,856	6.39
Superior parietal lobule left	−32	−53	52	2,654	8.61	1,453	5.31	—	n.s.	—	n.s.
Superior parietal lobule right	29	−42	44	1,354	7.56	79	4.36	—	n.s.	—	n.s.
Middle frontal gyrus left	−36	29	32	−520	−5.93	561	5.50	—	n.s.	—	n.s.
Middle frontal gyrus right	33	45	24	−10,122	−8.80	200	4.68	—	n.s.	—	n.s.
Lateral occ. gyri (ant. left)	−43	−65	−1		8.59	—	n.s.		6.27		n.s.
Lateral occ. gyri (ant. right)	39	−64	3		14.8	—	n.s.		6.85		n.s.
Lateral occ. gyri (mid. left)	−42	−78	7		14.5	—	n.s.		7.35		6.86
Lateral occ. gyri (mid. right)	34	−77	5		12.3	—	n.s.		6.78		5.75
Lateral occ. gyri (pos. left)	−13	−99	14		13.3	—	n.s.		7.81		7.21
Lateral occ. gyri (pos. right)	20	−91	21		12.4	—	n.s.		9.11		6.94
Precuneus (left and right)	5	−33	51	−20,091	−11.62	—	n.s.	—	n.s.		n.s.
Area striata (left and right)	−10	−72	11	−244,861	−19.24	30,305	6.82	−1,065	−6.41	1,967	7.24
Heschl's gyrus left	−37	−17	−4	−3,068	−7.49	—	n.s.	—	n.s.	—	n.s.
Heschl's gyrus right	39	−7	−0	−19,146	−9.54	—	n.s.	—	n.s.	—	n.s.

Note. For each comparison, the integral suprathreshold activation and the maximum Z score within a focus are given.

• Displaying squares (KS, NS) elicits a stronger activation of MCL and SMA than triangles (KT, NT). However, this effect is less pronounced compared to the target effect and the effect elicited by the Kanizsa figures. The posterior and middle parts of the lateral occipital gyri are also activated more strongly for square than for triangular stimuli. The periphery of AS is less suppressed, which might be explained by the larger spatial extent of the squares (Fig. 3, bottom).

• Kanizsa figures elicit a stronger activation of MCL and SMA than non-Kanizsa figures; however, this effect is less pronounced compared to the target effect in these areas. Kanizsa figures also activate the posterior and middle part of the lateral occipital gyri more strongly than nonillusory figures. This effect is seen in about the same areas where squares show stronger activations than triangles. In addition, Kanizsa figures lead to a stronger activation than non-Kanizsa figures in the anterior part of the lateral occipital gyrus (human motion area), where no activation was found for any other contrast (Fig. 3, third row).

Our experimental design does not allow a complete differentiation of target and figure processing, since the target shares the features of the standard figures. However, only a subset of areas was activated both by targets and by standards: MCL, SMA, and AS. These regions participate in the processing of all stimuli, due to the visual perception and motor response. Frontal, parietal, and extrastriate occipital regions were selectively activated by specific contrasts and allow the differentiation of exogenous processing, Gestalt processing, and target detection.

In summary, the activation increases in MCL and SMA for all conditions. The posterior and middle parts of the lateral occipital gyri exhibit a stronger activation for squares than for triangles and for Kanizsa figures than for non-Kanizsa figures. The anterior part of the lateral occipital sulcus is sensitive only to Kanizsa figures. The superior parietal lobes and the middle frontal gyri appear to be involved in the detection of targets. The periphery of AS is suppressed during stimulus display. This effect is less pronounced for squares and targets.

We now discuss results obtained from analyzing fMRI time courses by the nonlinear model according to Eq. (1). For each subject, ROI, and stimulus class, we obtained a relative gain (activation strength) and relative lag (time to response maximum). The mean lag time in AS was 4.88 ± 0.16 s (range 4.05–5.83 s). Resulting values were ordered by time and condition. Orderings were determined by computing Student's t tests (single sided, unequal variance, in which $>$ corresponds to $P < 0.05$, approximately to $P \geq 0.05$).

Results are summarized as follows:

• The temporal sequence of activations of ROIs and their mean relative lag were determined as MCL (−0.02 s) ~ AS (0.00 s) ~ POG (0.03 s) ~ MOG/AOG (0.11 s) < SMA (0.52 s) < SPL (+1.10 s). Three temporal activation groups are discriminated: (AS, POG, MOG/AOG, MCL) appear first, then SMA, and then SPL.

• Lag times for the target condition tended to be greater for the target condition in ROIs SPL (Δt = 0.38 s, $P = 0.079$) and SMA ($P = 0.056$), but not in the other ROIs.

• Relative gains vs experimental conditions were or-

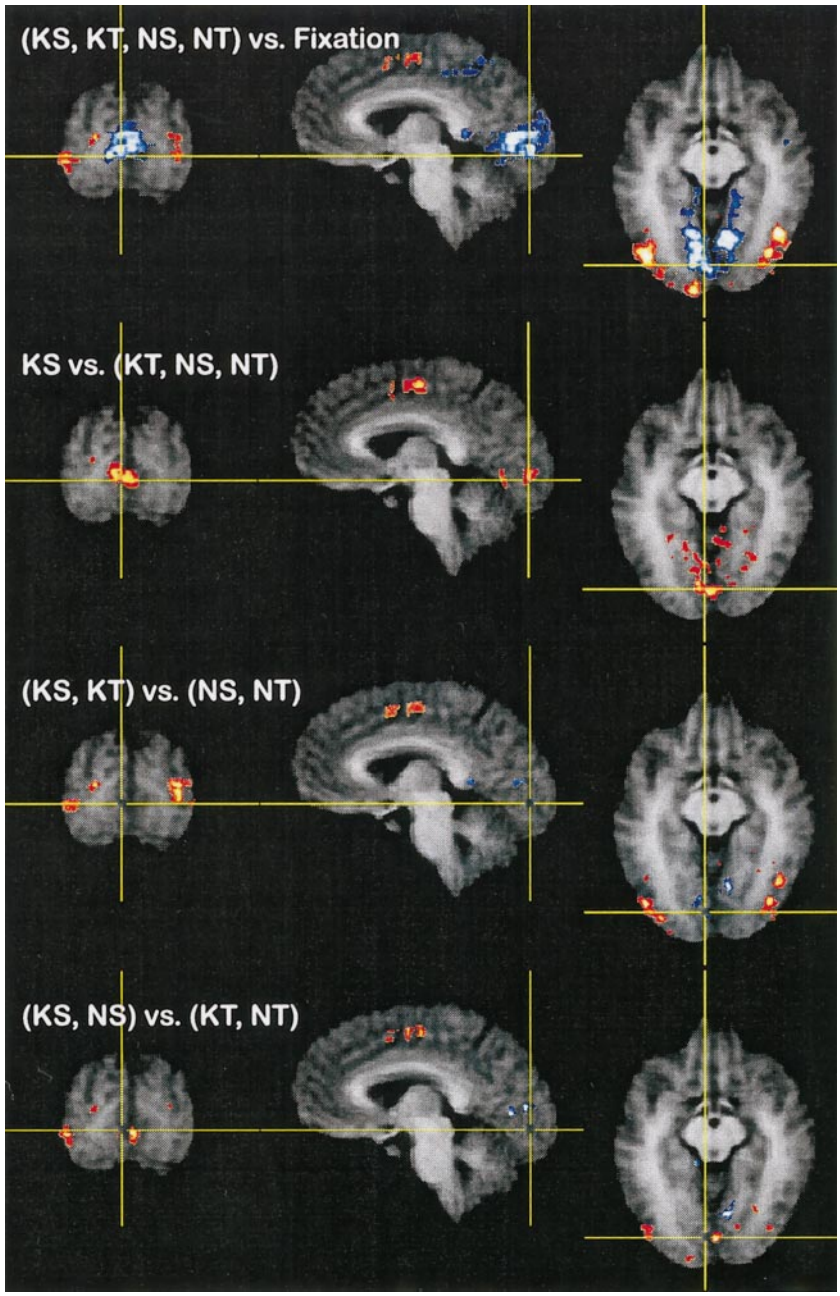

FIG. 3. Color-coded thresholded *Z*-score map ($|Z| \in [4;15]$), overlaid onto the group-averaged anatomical data set, which was transformed into Tailarach space. The top row corresponds to the evaluation of all conditions vs fixation, the second row to the target effect (KS vs (KT, NS, NT)), the third row to the effect of displaying Kanizsa figures ((KS, KT) vs (NS, NT)), the bottom row to the effect of displaying squares ((KS, NS) vs (KT, NT)). Activations are shown in a red-yellow color scale, deactivations in blue-white. Talairach coordinates and quantitative figures for areas are compiled in Table 2.

dered for all ROIs. We obtained a different order for the following ROIs: AS, KS ~ NS ~ KT ~ NS (equal for all conditions); POG/MOG/AOG, KS ~ KT > NT ~ NS (Kanizsa effect); and MCL, SMA, and SPL, KS > NT ~ KT ~ NS (target effect). While the activation of central portions of the striate cortex was independent of the stimulus, a stronger activation was found for Kanizsa figures in extrastriate occipital cortex. A clear selection of the target was found in ROIs MCL, SMA, and SPL. Activations in ROIs MFGL and MFGR were too low to warrant a proper modeling.

ERP Results

Grand-average event-related potentials for all four conditions are compiled in Fig. 4.

As apparent from Fig. 4, all stimuli evoked the typical P100 and N170 ERP responses. For statistical

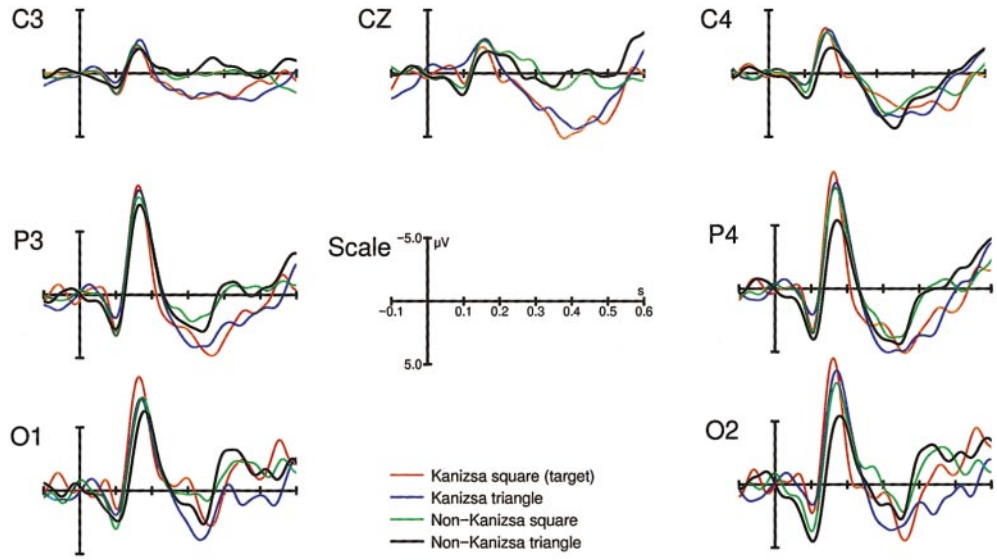

FIG. 4. ERPs recorded at six selected positions for the four conditions Kanizsa square, Kanizsa triangle, non-Kanizsa square, and non-Kanizsa triangle.

analysis, ERP amplitudes were pooled into six regions: left anterior (Fp1, F3), left central (C3, T3), left posterior (P3, O1), and their homologues on the right side. ERP components were defined by the time intervals 30–60 (N50), 70–110 (P100), 130–180 (N170), and 300–500 ms (P300). Repeated-measures ANOVAs with factors topography (anterior, central, posterior), hemisphere (left, right), and condition (KS, KT, NS, NT) were conducted to assess the effect of the experimental variables on the measured amplitudes.

For the N50 component the ANOVA revealed a significant effect of condition in both posterior regions ($F = 50.97$, $R^2 = 0.168$, $P < 1 \times 10^{-12}$), indicating that square figures elicited higher amplitudes than triangular ones. No effect was found for the other regions. Within the P100 time interval, the ANOVA also yielded a significant effect of condition ($F = 7.8$, $R^2 = 0.019$, $P = 0.05$). As might be inferred from Fig. 4, for the N170 component and both posterior regions, Kanizsa figures evoked larger N170 amplitudes: KS > KT > NS > NT ($F = 31.7$, $R^2 = 0.182$, $P < 1 \times 10^{-12}$). Likewise, the same ordering was found for the P300 component ($F = 13.3$, $R^2 = 0.022$, $P = 1 \times 10^{-8}$). All results are well in accordance with previous high-resolution ERP [17] and MEG [18] studies.

Results Discussion

We now try to summarize results from this combined ERP–fMRI study of a cognitive oddball task using illusory figures:

Exogenous Responses

ERP responses in the N50 and P100 time window from this and an earlier experiment [17] demonstrated a higher activation for squares than for triangles. This result is consistent with a slightly higher fMRI activation of the striate cortex found by the standard linear and the nonlinear regression model. We argue that this is due to that fact that the four Pac men, when flashed over the screen, lead to a greater change in overall brightness and have a greater spatial extent than only three of them; i.e., striate cortex and N50/P100 reflect exogenous processes sensitive to physical stimulus properties. The target effect of fMRI activation in striate cortex is probably not due to an early selection mechanism since early ERPs (N50, P100) do not show a target effect [16]. It is more likely that the striate cortex receives feedback from higher visual areas during a later stage of the selection [34].

Gestalt Perception

At a later processing stage (during the N170 time window), the amplitude ordering by condition changes to KS > KT > NS > NT, which is consistent with the regression results for the lateral occipital gyri. Therefore, we argue that N170 and extrastriate activation in the ventral visual path reflect endogenous processes of Gestalt perception. It has been shown recently that perception of an illusory figure enhanced visual N170 amplitude while the presence of collinear line segments alone did not lead to enhanced N170 amplitude, indicating that N170 reflects Gestalt perception [19]. The locations of the BOLD effect which resemble this effect in the lateral occipital gyri are in accordance with previous fMRI localization of the N170 sources [14].

Target Detection

Frontal and parietal areas (consisting of ROIs SPL and MFG bilaterally) are responsible for target detec-

tion: Both regions are more strongly activated comparing target to nontarget conditions in fMRI; this and previous EEG and MEG studies [17, 18] have demonstrated maxima of the P300 component over the centroparietal cortex (at positions P3 and P4) [17]. Frontal cortex and parietal or temporoparietal cortex have also been found responsible for P300 generation [33, 25, 24].

Response Generation

Similar to results from modeling other fMRI experiments [28, 30], ROIs SMA and MCL, which are responsible for response generation, are activated rather early and show a clearly stronger activation during target trials: KS > NT ~ KT ~ NS.

Attentional Modulation

The auditory cortex and periphery of the striate cortex are suppressed during stimulation. Most likely, suppression of auditory cortex reflects a cross-modality effect of shifting attention to the visual system while the suppression of peripheral striate cortex corresponds to an attentional focus within the visual modality on the cortical representation of the fovea where the stimuli were presented.

Unexpectedly, we found the anterior part of the lateral occipital gyri to be activated more strongly for Kanizsa figures than for non-Kanizsa figures. The Talairach coordinates of these areas (left, −43, −65, −1; right, 39, −64, 3) indicated a location close to the inferior temporal gyrus in Brodman area 37. This area has been localized as the human motion area MT [42, 15]. Human MT is sensitive not only to motion, but also to contrast, which is probably needed for motion detection [41]. Kanizsa figures induce an apparent brightness contrast, i.e., the illusory figure appears brighter than the physically identical brightness [10]. This could explain why Kanizsa figures activate human MT. In addition, it has been shown that sequential presentation of illusory figures at different positions induces very good apparent motion [35]. Therefore, it seems plausible to assume that the apparent brightness contrast induced by the illusory figure activates human MT, which in turn facilitates the perception of apparent motion.

Previous EEG recordings during fMRI scanning reported either EEG events such as alpha activity or spikes [22, 1, 2] or exogenous ERP components evoked by passive viewing of flickering checkerboards [3, 29, 4]. We were able to show that it is also possible to record ERPs during fMRI recording which go beyond exogenous responses, reflecting endogenous processes like Gestalt perception and target processing.

Our fMRI activations for Kanizsa figures in the posterior and middle part of the occipital gyri are well in accordance with previous findings [20, 36, 31]. However, the finding that illusory figures activate human MT was not previously reported, even though this area has been tested for an effect of Kanizsa figures [36].

DISCUSSION

The feasibility of recording ERPs during fMRI scanning using cognitive stimuli was demonstrated by recording ERPs with the expected configuration while measuring a typical pattern of BOLD responses. While the possibilities of this new methodology are exciting, a few issues should be remembered when planning such experiments, analyzing their data, or interpreting their results.

Problems of a Combined Measurement

There are mutual influences of the EEG and MRI measuring process. Our clustered EPI protocol allowed recording of five functional slices in 250 ms, but the EEG amplifier needed approximately 350 ms to recover from saturation. Thus, a window of 400 ms is lost for each block of scans from the EEG time course. For an average trial duration of 2.5 s here, this comprises an acceptable "duty cycle" of 84%. However, if the process under study requires scanning of a larger extent of the brain, this might leave EEG windows left which are too short for a meaningful evaluation.

The cardioballistic effect may be corrected by using one of the published methods [1, 2, 29]. Due to their comparatively high magnitude on our 3-T scanner, remnants of this artifact are still detectable in the corrected output, which corresponds to a lower SNR in the grand averages. We estimate that two to three times the trials of a conventional ERP experiment are needed in a combined EEG–fMRI measurement. To avoid picking up too much of this pulse-synchronous signal, we had to move the reference from the Goldmann point to the nasion. However, this drastically reduced the relative amplitude of the P300 component for the target condition.

Using 20 EEG electrodes and cables, which were radially joined at position Pz of the electrode cap, resulted in a loss of MR signal which was most noticeable in the topmost slices. This is best explained by a shielding effect of the cables and made the shimming process of the MR scanner tedious. Using this conventional EEG setup, this certainly poses an upper limit for the number of electrodes, most likely not much beyond 20. On the other hand, subjects did not report any adverse effects of a combined measurement.

Problems of Experimental Design

As stated above, the rather low SNR of the grand average forces one to design experiments with a rather high number of trials per class (say, at least 100). On the other hand, most details about the shape properties of the hemodynamic response are obtained when using rather long trial lengths (say, 12 s or more), so that the

overlap of sequential BOLD responses is negligible. Obviously, a compromise between the number of stimulus classes in a factorial (or parametric) design and the trial length must be made.

Here, we applied the rapid stimulation protocol using randomly varied trial length introduced by Burock *et al.* [7]. We presented 900 trials within 45 min, using a trial length of 2–3.5 s, and we were able to disentangle the class-wise properties of hemodynamic response by nonlinear regression analysis. Obviously, such rapid presentation is better suited to visual than to auditory stimulus material (e.g., read-out sentences).

A greater freedom in experimental design is possible when improving the SNR of ERP acquisition to a level comparable to separate measurements. An improved subject setup and advances in sensor and amplifier construction are expected to yield the most benefit. Because artifacts scale supralinearly with field strengths, it might even be beneficial to conduct such experiments at 1.5-T field strengths, sacrificing sensitivity for the BOLD signal in favor of a less-distorted EEG.

Problems of Analyzing Data

We analyzed measured EEG and fMRI data in a conventional fashion, i.e., each measurement separately. When trying to create a synthesis of the results for ERP and fMRI data analysis, the following physiological response properties must be remembered: ERPs measured on the scalp have a rather low spatial resolution, which is partially due to a spatial low-pass filtering effect of the outer hulls of the brain, and thus correspond to an integral activation of a certain brain region at a given time point. Conversely, the BOLD response may be understood as a (fast) neuronal activation convolved by a (slow) hemodynamic response function. This corresponds to a low-pass filtering effect in time or an integral activation over a certain time window at a specific brain location. In addition, it is still unclear to what extent lag times are influenced by a delay in neuronal activation *or* in delivery of oxygenated blood to the response area.

Unique models about the underlying processes involved in a cognitive task may be constructed, assuming that processes are strictly sequential in time and well separated in space. While this assumption may approximately hold for early processing stages (i.e., during stimulus perception), it is well known that later processing stages (i.e., decision-making, response generation) require a network of temporally strongly overlapping processes, in which even reactivations of certain brain regions are under discussion [34]. Modeling such a network will most likely yield nonunique solutions.

The above qualitative hypothetical model for processing Kanizsa figures is in accordance with experimental findings from this combined and previous separate measurements. It implicitly reflects an underlying hypothesis that the absolute ERP amplitudes correspond to fMRI activation strengths, although there is no strict experimental evidence for this assumption. Even within limits as discussed above, a lot of perspectives are open for performing similar experiments using higher level cognitive tasks. The perspective of observing complementary responses from the same stimulation event on a single-subject level is very appealing in order to better understand physiological processes underlying brain activation and the functional organization of the brain.

REFERENCES

1. Allen, P. J., Polizzi, G., Krakow, K., Fish, D. R., and Lemieux, L. 1998. Identification of EEG events in the MR scanner: The problem of pulse artifact and a method for its subtraction. *NeuroImage* **8:** 229–239.
2. Allen, P. J., Josephs, O., and Turner, R. 2000. A method for removing imaging artifact from continuous EEG recorded during functional MRI. *NeuroImage* **12:** 230–239.
3. Bonmassar, G., Anami, K., Ives, J., and Belliveau, J. W. 1999. Visual evoked potential (VEP) measures by simultaneous 64-channel EEG and 3T fMRI. *NeuroReport* **10:** 1893–1897.
4. Bonmassar, G., Schwartz, D. P., Liu, A. K., Kwong, K. K., Dale, A. M., and Belliveau, J. W. 2001. Spatiotemporal brain imaging of visual-evoked activity using interleaved EEG and fMRI recordings. *NeuroImage* **13:** 1035–1043.
5. Buckner, R. L., Bandettini, P. A., O'Craven, K. M., Savoy, R., Petersen, S. E., Raichle, M., and Rosen, B. 1996. Detection of transient and distributed cortical activation during averaged single trials of a cognitive task using functional magnetic resonance imaging. *Proc. Natl. Acad. Sci. USA* **93:** 14878–14883.
6. Buckner, R. L. 1998. Event-related fMRI and the hemodynamic response. *Hum. Brain Mapp.* **6:** 373–377.
7. Burock, M. A., Buckner, R. L., Woldorff, M. G., Rosen, B. R., and Dale, A. M. 1998. Randomized event-related experimental designs allow for extremely rapid presentation rates using functional MRI. *NeuroReport* **9:** 3735–3739.
8. Chiappa, K. H., Huang-Hellinger, F., Jenkins, B. G., and Hill, R. A. 1995. EEG during MR imaging: Differentiation of movement artifact from paroxysmal cortical activity. *Neurology* **45:** 1942–1943.
9. Clark, V. P., Maisog, J. M., and Haxby, J. V. 1998. FMRI study of face perception and memory using random stimulus sequences. *J. Neurophysiol.* **79:** 3257–3265.
10. Dresp, B., Lorenceau, J., and Bonnet, C. 1990. Apparent brightness enhancement in the Kanizsa square with and without illusory contour formation. *Perception* **19:** 483–489.
11. Friston, K. J., Worsley, K. J., Frackowiak, R. S. J., Mazziotta, J. C., and Evans, A. C. 1994. Assessing the significance of focal activations using their spatial extent. *Hum. Brain Mapp.* **1:** 210–220.
12. Friston, K. J., Williams, S., Howard, R., Frackowiak, R. S. J., and Turner, R. 1996. Movement-related effects in fMRI time series. *Magn. Reson. Med.* **35:** 346–355.
13. Goldman, R. I., Stern, J. M., Engel, J., and Cohen, M. S. 2000. Acquiring simultaneous EEG and functional MRI. *Clin. Neurophysiol.* **111:** 1974–1980.
14. Gomez Gonzales, C. M., Clark, V. P., Fan, S., Luck, S. J., and Hillyard, S. A. 1994. Sources of attention-sensitive visual event-related potentials. *Brain Topogr.* **7:** 41–51.

15. Hasnain, M. K., Fox, P. T., and Woldorff, M. G. 1998. Intersubject variability of functional areas in the human visual cortex. *Hum. Brain Mapp.* **6:** 301–315.
16. Heinze, H. J., Mangun, G. R., Bruchert, W., Hinrichs, H., Scholz, M., Münte, T. F., Gös, A., Johannes, S., Scherg, M., Hundeshagen, H., Gazzaniga, M. S., and Hillyard, S. A. 1994. Combined spatial and temporal imaging of spatial selective attention in humans. *Nature* **392:** 543–546.
17. Herrmann, C. S., Mecklinger, A., and Pfeifer, E. 1999. Gamma responses and ERPs in a visual classification task. *Clin. Neurophysiol.* **110:** 636–642.
18. Herrmann, C. S., Mecklinger, A., and Pfeifer, E. 2000. Magnetoencephalographic responses to illusory figures: Early evoked gamma is affected by processing of stimulus features. *Int. J. Psychophysiol.* **38:** 265–281.
19. Herrmann, C. S., and Bosch, V. 2001. Gestalt perception modulates early visual processing. *NeuroReport* **12:** 901–904.
20. Hirsch, J., DeLaPaz, R. L., Relkin, N. R., Victor, J., Kim, K., Li, T., Borden, P., Rubin, N., and Shapley, R. 1995. Illusory contours activate specific regions in human visual cortex: Evidence from functional magnetic resonance imaging. *Proc. Natl. Acad. Sci. USA* **92:** 6469–6473.
21. Huang-Hellinger, F., Breiter, H. C., McCormack, G., Cohen, M. S., Kwong, K. K., Sutton, J. P., Savoy, R. L., Weisskopf, R. M., Davis, T. L., Baker, J. R., Belliveau, J. W., and Rosen, B. R. 1995. Simultaneous functional magnetic resonance imaging and electrophysiological recording. *Hum. Brain Mapp.* **3:** 13–23.
22. Ives, R. J., Warach, S., Schmitt, F., Edelmann, R. R., and Schmoer, D. L. 1993. Monitoring the patient's EEG during echo planar MRI. *Electroencephogr. Clin. Neurophysiol.* **87:** 417–420.
23. Josephs, O., and Henson, R. N. A. 1999. Event-related functional magnetic resonance imaging: Modelling, inference and optimization. *Philos. Trans. R. Soc. London* **354:** 1215–1228.
24. Kirino, E., Belger, A., Goldman-Rakic, P., and McCarthy, G. 2000. Prefrontal activation evoked by infrequent target and novel stimuli in a visual target detection task: An event-related functional magnetic resonance imaging study. *J. Neurosci.* **20:** 6612–6618.
25. Knight, R. T., Scabini, D., Woods, D. L., and Clayworth, C. C. 1989. Contributions of temporal–parietal junction to the human auditory P3. *Brain Res.* **502:** 109–116.
26. Krakow, K., Allen, P. J., Symms, M. R., Lemieux, L., Josephs, O., and Fish, D. R. 2000. EEG recording during fMRI experiments: Image quality. *Hum. Brain Mapp.* **10:** 10–15.
27. Kruggel, F., von Cramon, D. Y., and Descombes, X. 1999. Comparison of filtering methods for fMRI datasets. *NeuroImage* **10:** 530–543.
28. Kruggel, F., and von Cramon, D. Y. 1999. Modeling the hemodynamic response in single-trial functional MRI experiments. *Magn. Reson. Med.* **42:** 787–797.
29. Kruggel, F., Wiggins, C. J., Herrmann, C. S., and von Cramon, D. Y. 2000. Recording of the event-related potentials during functional MRI at 3.0 Tesla field strength. *Magn. Reson. Med.* **44:** 277–282.
30. Kruggel, F., Zysset, S., and von Cramon, D. Y. 2000. Nonlinear regression of functional MRI data: An item recognition task study. *NeuroImage* **12:** 173–183.
31. Larsson, J., Amunts, K., Gulyas, B., Malikovic, A., Zilles, K., and Roland, P. E. 1999. Neuronal correlates of real and illusory contour perception: Functional anatomy with PET. *Eur. J. Neurosci.* **11:** 4024–4036.
32. Lemieux, L., Allen, P. J., Franconi, F., Symms, M. R., and Fish, D. R. 1997. Recording of EEG during fMRI experiments: Patient safety. *Magn. Reson. Med.* **38:** 943–952.
33. Linden, D. E., Prvulovic, D., Formisano, E., Vollinger, M., Zanella, F. E., Goebel, R., and Dierks, T. 1999. The functional neuroanatomy of target detection: An fMRI study of visual and auditory oddball tasks. *Cereb. Cortex* **9:** 815–823.
34. Martinez, A., Anllo-Vento, L., Sereno, M. I., Frank, L. R., Buxton, R. B., Dubowitz, D., Wong, E. C., Hinrichs, H., Heinze, H. J., and Hillyard, S. A. 1999. Involvement of striate and visual cortical areas in spatial attention. *Nat. Neurosci.* **2:** 364–369.
35. Mather, G. 1988. Temporal properties of apparent motion in subjective figures. *Perception* **17:** 729–736.
36. Mendola, J. D., Dale, A. M., Fischl, B., Liu, A. K., and Tootell, R. B. 1999. The representation of illusory and real contours in human cortical visual areas revealed by functional magnetic resonance imaging. *J. Neurosci.* **19:** 8560–8572.
37. Müri, R. M., Felbinger, J., Rösler, K. M., Jung, B., Hess, C. W., and Boesch, C. 1998. Recording of electrical brain activity in a magnetic resonance environment: Distorting effects of the static magnetic field. *Magn. Reson. Med.* **39:** 18–22.
38. Opitz, B., Mecklinger, A., von Cramon, D. Y., and Kruggel, F. 1999. Combining electrophysiological and hemodynamic measures of the auditory oddball. *Psychophysiology* **36:** 142–147.
39. Press, W. H., Teukolsky, S. A., Vetterling, W. T., and Flannery, B. P. 1992. Numerical recipes in C, 2nd ed. Cambridge Univ. Press, Cambridge, UK.
40. Richter, W., Andersen, P., Georgopoulos, A. P., and Kim, S. G. 1997. Sequential activity in human motor areas during a delayed cued finger movement task studied by time-resolved fMRI. *NeuroReport* **8:** 1257–1261.
41. Tootell, R. B., Reppas, J. B., Kwong, K. K., Malach, R., Born, R. T., Brady, T. J., Rosen, B. R., and Belliveau, J. W. 1995. Functional analysis of human MT and related visual cortical areas using magnetic resonance imaging. *J. Neurosci.* **15:** 3215–3230.
42. Watson, J. D., Myers, R., Frackowiak, R. S., Hajnal, J. V., Woods, R. P., Mazziotta, J. C., Shipp, S., and Zeki, S. 1993. Area V5 of the human brain: Evidence from a combined study using positron emission tomography and magnetic resonance imaging. *Cereb. Cortex* **3:** 79–94.
43. Woldorff, M. G., Tempelmann, C., Fell, J., Tegeler, C., Gaschler-Markefski, B., Hermann, H., Heinze, H. J., and Scheich, H. 1999. Lateralized auditory spatial perception and the contralaterality of cortical processing as studied with fMRI and MEG. *Hum. Brain Mapp.* **7:** 49–66.
44. Worsley, K. J., and Friston, K. J. 1996. Analysis of fMRI time-series revisited—Again. *NeuroImage* **2:** 173–181.